Influence of Fluid Dynamics on Heat Transfer in a Preswirl Rotating-Disk System

Gary D. Lock

Michael Wilson

J. Michael Owen

Department of Mechanical Engineering,
University of Bath,
Bath BA2 7AY, UK

Modern gas turbines are cooled using air diverted from the compressor. In a "direct-transfer" preswirl system, this cooling air flows axially across the wheel space from stationary preswirl nozzles to receiver holes located in the rotating turbine disk. The distribution of the local Nusselt number Nu on the rotating disk is governed by three nondimensional fluid-dynamic parameters: preswirl ratio β_p*, rotational Reynolds number* Re_ϕ*, and turbulent flow parameter* λ_T*. This paper describes heat transfer measurements obtained from a scaled model of a gas turbine rotor-stator cavity, where the flow structure is representative of that found in the engine. The experiments reveal that Nu on the rotating disk is axisymmetric except in the region of the receiver holes, where significant two-dimensional variations have been measured. At the higher coolant flow rates studied, there is a peak in heat transfer at the radius of the preswirl nozzles associated with the impinging jets from the preswirl nozzles. At lower coolant flow rates, the heat transfer is dominated by viscous effects. The Nusselt number is observed to increase as either* Re_ϕ *or* λ_T *increases.* [DOI: 10.1115/1.1924721]

1 Introduction

The specific work of gas turbines increases with higher gas temperature, and typical modern engines experience turbine entry temperatures (TET) of up to 1800 K. At these elevated temperatures, the turbine components (disks, nozzle guide vanes, and rotor blades) require cooling for safe operation and acceptable lifetime. Increasing the mass flow rate of coolant allows an increase in the TET, which is the main objective of using cooling flow. However, effective turbine cooling incurs a thermodynamic cost: first, the compressed air is diverted from the main flow and not used in combustion; second, there are coolant pressure losses in the feed, delivery, and blade passages; and third, the viscous mixing of coolant with the mainstream after ejection will reduce the aerodynamic efficiency of the turbine. The engine designer has the task of creating a coolant system that optimizes the specific fuel consumption, using a compromise between increased TET and this reduced turbine efficiency.

Preswirl nozzles are often used in gas turbines to deliver the cooling air to the turbine blades, as illustrated in Fig. 1. The stationary nozzles swirl the cooling air in the direction of rotation of the turbine disk, thereby reducing the temperature of the air relative to the blades. The designer needs to know the effect of the preswirl ratio β_p, the coolant flow rate, and the rotational speed Ω on the pressure drop and temperature difference between the preswirl nozzles and the receiver holes in the disk. It is also important to know the effect of these parameters on the distribution of Nusselt number Nu over the surface of the rotating disk.

Designers can obtain some information using turbine-based rigs running close to engine-operating conditions. However, deeper insight can be gained from fundamental research which measures, computes and explains the flow and heat transfer in generic, fully-instrumented rigs operating under more benign conditions. Computational codes, validated on these detailed measurements, can then be used to conduct calculations extrapolated to engine conditions.

Owen and Rogers [1], Karabay et al. [2], and Pilbrow et al. [3] presented experimental and computational results for flow and heat transfer in a "cover-plate" (rotating cavity) preswirl system, showing that the structure of these flows is governed principally by the values of β_p and the turbulent-flow parameter, $\lambda_T = C_w\,\mathrm{Re}_\phi^{-0.8}$. (The turbulent flow parameter, which combines the effects of the nondimensional preswirl flow rate C_w and the rotational Reynolds number Re_ϕ for the disk, is related to the entrainment of fluid into the boundary layer on a rotating disk; for turbulent flow, $\lambda_T \approx 0.22$ for the entrainment due to an unconfined disk [3].) The heat transfer is governed by the above two parameters as well as by the rotational Reynolds number Re_ϕ and by the temperature distribution on the rotating disk.

This paper discusses the effects of β_p, λ_T, and Re_ϕ on the heat transfer between the air and the rotating disk in a generic rig. The experimental facility is a simplified model of a gas turbine rotor-stator system designed to accommodate pressure and temperature instrumentation in the test section and to provide optical access to the wheel-space.

Meierhofer and Franklin [4] were the first to experimentally confirm the significant reduction in relative total temperature using a preswirl system and quantified the effectiveness of such a system in terms of the ratio of delivery air velocity to disk speed. Extensive research is currently being conducted at the University of Karlsruhe: Dittmann et al. [5,6] have reported the discharge behavior and Geis et al. [7] have reported measurements of temperature reduction in preswirl systems. Chew et al. [8] presented a theoretical analysis to determine cooling air delivery temperatures, which was shown to correlate well with experimental measurements.

2 Experimental Apparatus

Experiments were conducted using a scaled model of a gas-turbine rotor-stator system. The geometry, which was based on information obtained for existing engine designs, is illustrated schematically in Fig. 2. The air entered the test section through the stator at low radius via preswirl nozzles and flowed radially out-

Contributed by the International Gas Turbine Institute (IGTI) of THE AMERICAN SOCIETY OF MECHANICAL ENGINEERS for publication in the ASME JOURNAL OF ENGINEERING FOR GAS TURBINES AND POWER. Paper presented at the International Gas Turbine and Aeroengine Congress and Exhibition, Vienna, Austria, June 13–17, 2004, Paper No. 2004-GT-53158. Manuscript received by IGTI, October 1, 2003; final revision, March 1, 2004. IGTI Review Chair: A. J. Strazisar.

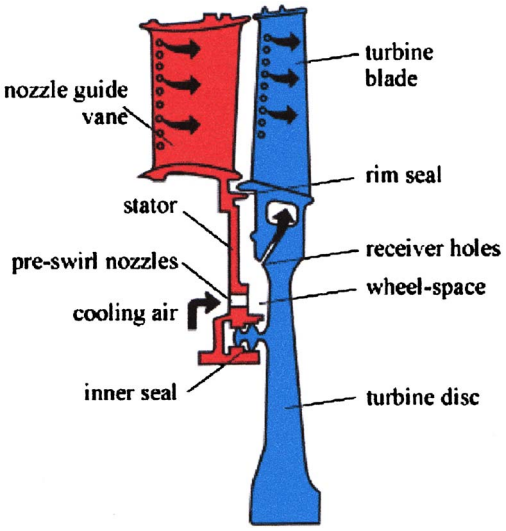

Fig. 1 Simplified diagram of typical pre-swirl cooling-air system for a gas turbine

ward between the rotating disk and the stator, exiting through receiver holes in the rotating disk representing the entrance to the blade-cooling passages in the engine.

The disk radius was $b=216$ mm, and the other principal dimensions are the inner-to-outer radius ratio $a/b=0.67$ and the gap ratio $s/b=0.051$. The stator was machined from aluminum and contained 24 circular preswirl nozzles angled at 20 deg to the tangential direction. The rotating disk was machined from transparent polycarbonate, with sectors sprayed with thermochromic liquid crystals (TLC) and black paint, and contained 60 axial receiver holes with a length-to-diameter ratio of 1.25. The nondimensional radius of the nozzles, $x_p=r_p/b=0.74$, was less than that of the receiver holes, $x_b=r_b/b=0.93$, and the area ratio of the receiver holes to that of the nozzles was 2.9.

A cross-sectional drawing of the working section is shown in Fig. 3, identifying the different materials used in the construction of the apparatus. A small flow of air was passed through an annular chamber to seal the periphery. All mass flow rates were measured using a standard orifice plate.

The disk could be rotated up to speeds of 5000 rpm, providing a maximum rotational Reynolds numbers Re_ϕ (based on disk radius) up to 1.2×10^6. This value is typically an order of magnitude less than those found in gas turbines. The mass flow rates were chosen to simulate engine-representative values of β_p and λ_T and, as discussed above, the flow structure within the rotating cavity depends principally on these two parameters and only weakly on

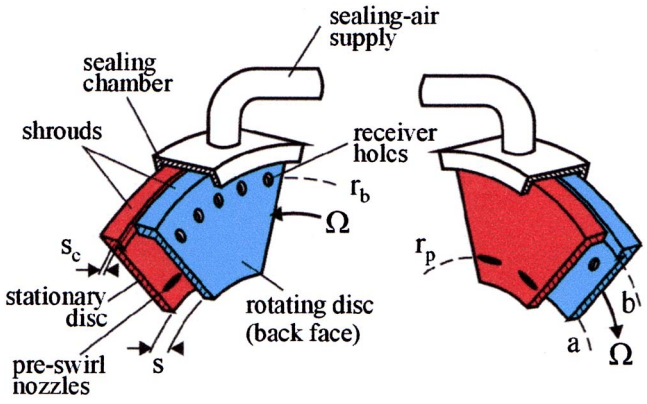

Fig. 2 Schematic diagram of test-section geometry

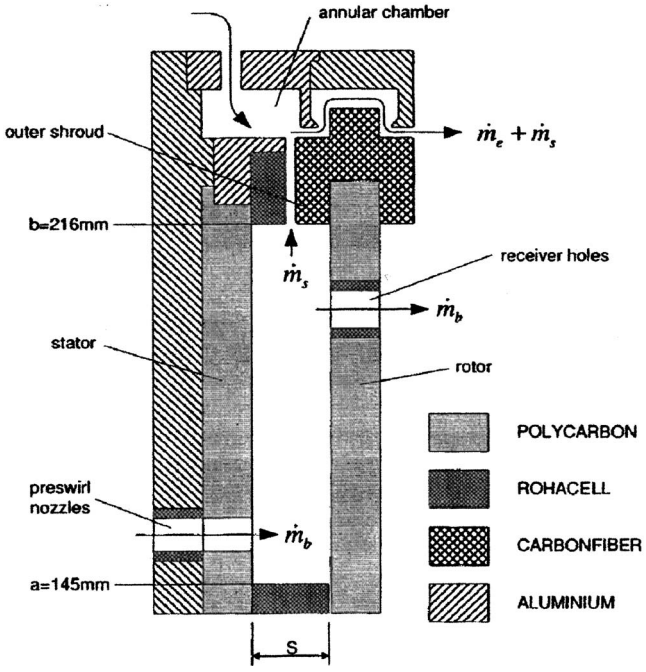

Fig. 3 Cross-sectional drawing of test rig

Re_ϕ. Hence the flow structure is considered to be representative of that found in cooling systems of engines. Experiments were conducted for around 20 test conditions covering the following parametric range: $0.78\times10^6<\mathrm{Re}_\phi<1.2\times10^6$; $0.125<\lambda_T<0.36$; $0.5<\beta_p<1.5$. The geometric properties and operating conditions are summarized in Table 1.

The number of preswirl nozzles N could be reduced from $N=24$ to 12 by blocking every other nozzle, and this allowed higher inlet swirl ratios to be tested for the preswirl flow rates available. The ratio of the area of the receiver holes to that of the nozzles was 2.9 for $N=24$ and 5.8 for $N=12$. The design of the rig did not allow independent testing of β_p and λ_T. The inlet swirl ratio β_p was calculated from

$$\beta_p=\frac{C}{N}\left(\frac{C_{W,p}}{\mathrm{Re}_\phi}\right)=\frac{C}{N}\lambda_T\,\mathrm{Re}_\phi^{-0.2}$$

where

$$C=\frac{4b^3\cos\theta}{\pi d^2 r_p}$$

for preswirl nozzles of diameter d and tangential angle θ.

The fluid dynamics of this facility has been investigated both experimentally and computationally by Yan et al. [9]. The effects of rotational speed, flow rate, preswirl ratio, and the number of preswirl nozzles on the flow field and on the total pressure losses in the system have been reported. These measurements and computations showed that there was a significant loss of total pressure

Table 1 Summary of geometry and operating conditions

Disk radius, b	216 mm
Inner radius, a	$a/b=0.67$
Gap, s	$s/b=0.051$
Preswirl radius	$r_p/b=0.74$
Receiver-hole radius	$r_b/b=0.93$
Re_ϕ	$0.78-1.2\times10^6$
λ_T	0.125–0.36
β_p	0.5–1.5

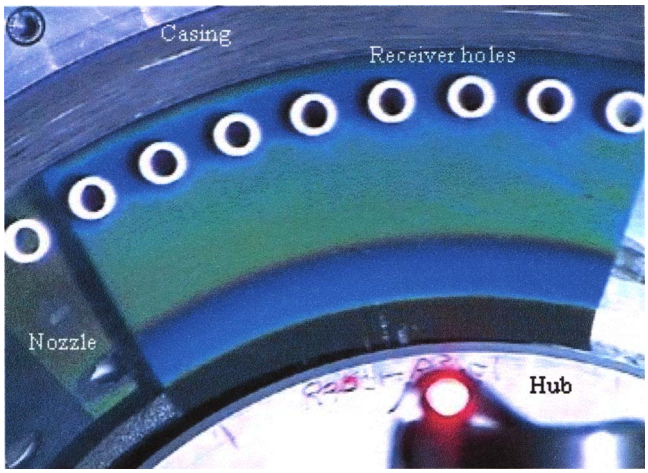

Fig. 4 Video image of TLC on rotating disk. Color photograph available in ASME Paper 2004-GT-53158.

between the outlet from the preswirl nozzles and the rotating core of fluid in the wheel space. This loss increased as the preswirl flow rate and inlet swirl ratio increased and as the number of nozzles decreased. The discharge coefficient of the receiver holes increased as the preswirl ratio at the receiver-hole radius approached unity. (Information concerning discharge coefficients is given in the Appendix.)

3 Heat Transfer Experiments

Local heat transfer coefficients on the rotating disk were determined from transient surface-temperature measurements using thermochromic liquid crystals (TLC), as described by Lock et al. [10]. These experiments were conducted under known thermal boundary conditions, using air that had been preheated to approximately 60°C using a mesh heater upstream of the preswirl nozzles. The measurements relied on the accurate measurement of the time taken for 30°C and 40°C narrow-band TLC on the rotor surface to reach a unique value of hue, which had been calibrated against temperature. The crystals were sprayed on the disk in sectors inside the wheel space, which could be viewed through the transparent polycarbonate by a digital video camera, running at 25 fps, under the illumination of a strobe light synchronized to the disk frequency. A thin layer of black paint was used to provide contrast to the color play of the TLC.

Figure 4, taken from Lock et al. [10], is a color image selected from a time sequence obtained by the digital camera during a typical experiment. This image shows the color play of the TLC as viewed through the transparent polycarbonate disk. Initially clear when below its activation temperature, the TLC changed color from red to green to blue as the disk was heated by the hot gas entering through the preswirl nozzles. The image appears "frozen" because the rotor was illuminated by the stroboscopic light synchronized with the disk rotating at 5000 rpm.

The hub and casing, at radii a and b, are marked in Fig. 4. The blade receiver holes, insulated using low-conductivity, white-colored rohacell foam, are also labeled. The narrow-band TLC and overcoat of black paint had been sprayed in a 48 deg sector on the disk covering eight of the 60 receiver holes. To the left of this painted sector the stator, coated with wideband TLC, two of the 24 preswirl nozzles are visible through the transparent (unpainted) polycarbonate at low radius. Some shadows appear around the receiver holes because of constraints with the lighting and viewing angles.

In Fig. 4 both the 30°C and 40°C narrow-band TLC have been activated into their visible range and display different colors at different locations on the rotating disk. Blue reveals higher temperature, indicating that there is a region of relatively high heat transfer around the receiver holes. The virtually identical TLC patterns around each of these holes indicate the periodicity of the flow structure. Note that the stator, as indicated by the change in color of the wideband TLC, has also been heated throughout this transient process.

Color images (typically 800×600 pixels), recorded at 25 fps by the digital camera, were subsequently converted to hue. It was then possible to obtain the hue history of each pixel in the image and, hence, the time taken for the surface to reach a prescribed value of hue.

The air total temperature was measured using fast-response thermocouple probes in the preswirl cavity. These probes and the TLC calibration are described by Lock et al. [10].

4 Data Analysis

The heat transfer coefficient h is defined as

$$q_w = h(T_{aw} - T_w) \tag{4.1}$$

where q_w is the surface heat flux from the air to the wall, T_w is the surface temperature of the wall, and T_{aw} is the adiabatic-wall temperature. T_{aw} depends on the total temperature of the air T_a and on the fluid dynamics.

In a typical transient test, an abrupt change in air temperature is generated and narrow-band TLC is used to determine the surface temperature T_w of the test piece. Knowing the time t at which the surface reaches T_w, h (assumed time-invariant) can be calculated from the solution of Fourier's one-dimensional conduction equation for the case of a semi-infinite plate.

In the tests reported here, the mesh heater created an effective step change in the air temperature, but at the test section an exponential-type of behavior (or so-called slow transient) was produced. Lock et al. [10] show that the adiabatic wall temperature T_{aw} could be fitted by an exponential series of m terms, such that

$$T_{aw}(t) = T_{a,0} + \sum_{j=1}^{m} T_{a,j}(1 - e^{-t/\tau_j}) + F \tag{4.2}$$

where $T_{a,0}$ is the air temperature at $t=0$, $T_{a,j}$ and τ_j are the constant amplitudes and time constants, respectively and F is a time-invariant parameter that depends on the fluid dynamics.

As $t\to\infty$,

$$T_{aw,\infty} = T_0 + \sum_{j=1}^{m} T_{a,j} \tag{4.3}$$

where T_0 is the initial temperature of the wall, such that

$$T_0 = T_{a,0} + F \tag{4.4}$$

Fourier's conduction equation for a semi-infinite slab has been solved by Gillespie et al. [11] for the case where there is a simple exponential increase in the air temperature, corresponding to the case where $m=1$ in Eq. (4.3). The solution is

$$\Theta = \frac{T_w - T_0}{T_{aw,\infty} - T_0} = g(\beta, \beta_\tau) \tag{4.5}$$

where

$$g(\beta,\beta_\tau) = 1 - \frac{1}{1+\beta_\tau^2} e^{\beta^2}\,\mathrm{erfc}(\beta) - e^{-t/\tau}\frac{\beta_\tau^2}{1+\beta_\tau^2} \times \left\{ 1 + \frac{1}{\beta_\tau}\left[\frac{1}{\pi}\sqrt{\frac{t}{\tau}} + \frac{2}{\pi}\sum_{n=1}^{\infty}\frac{1}{n} e^{-\pi^2/4}\sinh\left(n\sqrt{\frac{t}{\tau}}\right)\right]\right\} \tag{4.6}$$

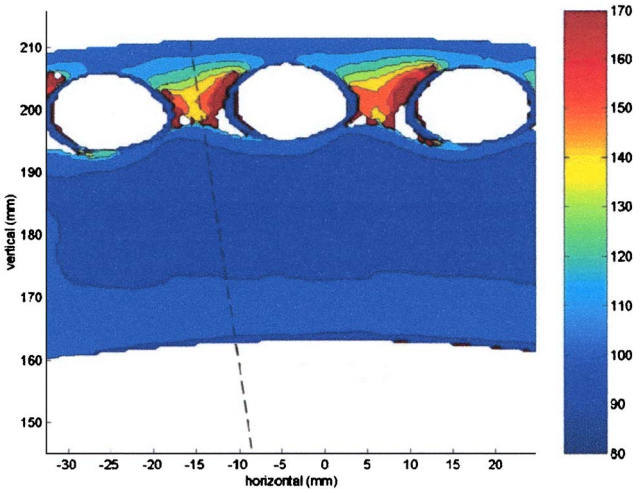

Fig. 5 Contour map of heat transfer coefficient (W/m²K) for viscous dominated flow: $Re_\phi \approx 0.8\times10^6$, $\lambda_T \approx 0.125$, $\beta_p \approx 0.5$. The disk is rotating counter-clockwise. Color contours available in ASME Paper 2004-GT-53158.

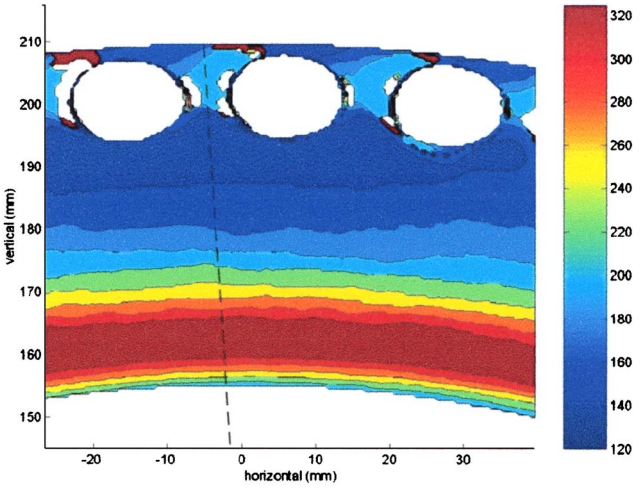

Fig. 6 Contour map of heat transfer coefficient (W/m²K) for inertially dominated flow: $\lambda_T \approx 0.36$, $\beta_p \approx 1.4$, $Re_\phi \approx 0.8\times10^6$. Counter-clockwise rotation. Color contours available in ASME Paper 2004-GT-53158.

$$\beta = \frac{h\sqrt{t}}{\sqrt{\rho c k}} \tag{4.7}$$

and

$$\beta_\tau = \frac{h\sqrt{\tau}}{\sqrt{\rho c k}} \tag{4.8}$$

For the case where $\tau=0$, Eq. (4.5) simplifies to

$$\Theta = f(\beta) \tag{4.9}$$

where, from Eq. (4.6),

$$f(\beta) = 1 - e^{\beta^2}\,\mathrm{erfc}(\beta) \tag{4.10}$$

which is the well-known solution of Fourier's equation for a step change in the air temperature.

The general solution for an exponential series, corresponding to Eq. (4.3), is given by Newton et al. [12] as

$$\Theta = \sum_{j=1}^{m} \frac{T_{a,j}}{T_{aw,\infty} - T_0} g(\beta, \beta_{\tau_j}) \tag{4.11}$$

For the special case where $m=1$, $T_{a,1}=T_{aw,\infty}-T_0$ and Eq. (4.11) reduces to (4.6).

5 Two-Dimensional Experimental Results

Figures 5 and 6 are typical contour maps of heat transfer coefficient on the rotating disk. The data were collected from experiments conducted at the same Re_ϕ, but different values of β_p and λ_T and the different flow structures have created markedly different heat transfer patterns. The data are based on the 40°C narrow-band TLC.

The fluid dynamic conditions for Fig. 5 feature a relatively low value of λ_T, hence relatively weak impingement from the preswirl nozzles, and this "viscous" flow regime is dominated by the boundary layer on the rotating disk. The largest levels of h are measured near the receiver holes. These holes have created three-dimensional flow near the surface of the disk, which, in turn, leads to the two-dimensional distribution of h in their vicinity. Away from this region there is little radial or circumferential variation in h.

The fluid dynamic conditions for Fig. 6 feature a relatively high value of λ_T, hence relatively high-velocity jets exiting the preswirl nozzles, and this "inertial" flow regime is dominated by impingement on the rotating disk. There is a strong radial variation in h, with the highest levels located at the nozzle radius ($x=0.74$); there is also a smaller peak near the receiver holes. The h contours show little circumferential variation away from this vicinity.

6 Radial Variation of Nusselt Number

Lock et al. [10] presented two-dimensional distributions of local Nusselt number over the rotating disk surface for different test conditions. In all cases these exhibited nearly axisymmetric behavior, except in regions near and around the receiver holes. There was generally good repeatability for measurements obtained between different pairs of holes. This section will discuss how the governing fluid dynamic parameters, Re_ϕ, λ_T, and β_p, and the number of nozzles N effect the Nusselt number distribution.

Effect of λ_T and β_p at Constant Re_ϕ and $N=24$. Figures 7 and 8 illustrate, respectively, the effect of varying λ_T (and as a consequence, of varying β_p) on the measured radial variation of Nu for $Re_\phi=0.8\times10^6$ and 1.2×10^6. The measurements correspond to radial lines midway between the receiver holes (see the dotted line in Figs. 5 and 6).

At both Reynolds numbers the Nusselt number variation with x is characterized by viscous behavior at low values of $\lambda_T=0.12$

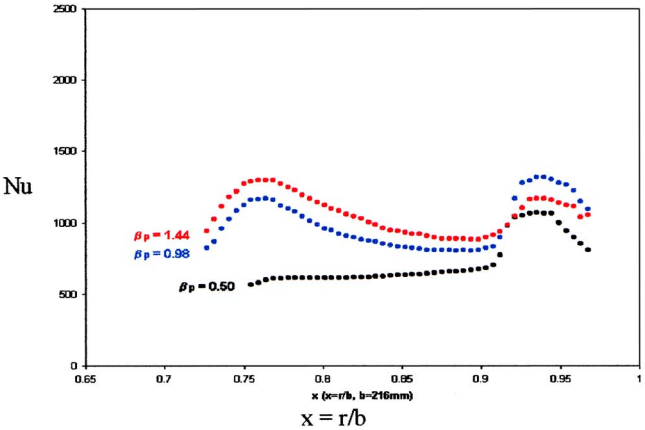

Fig. 7 Effect of λ_T and β_p on the radial distribution of Nu: $Re_\phi \approx 0.8\times10^6$

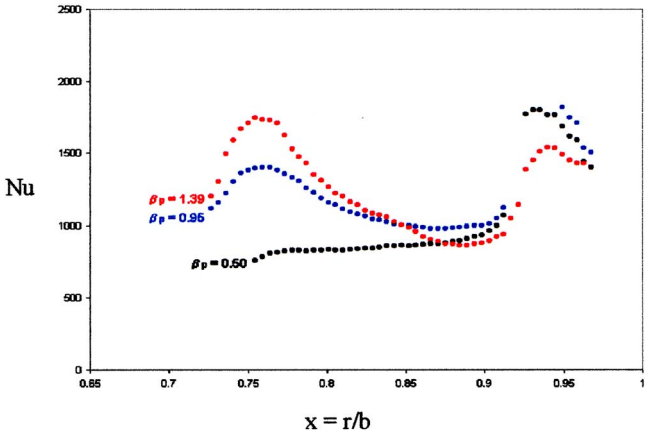

Fig. 8 Effect of λ_T and β_p on the radial distribution of Nu: $Re_\phi \approx 1.2 \times 10^6$

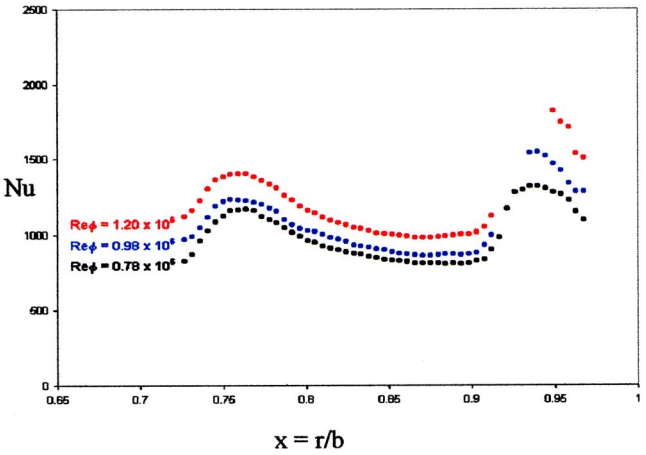

Fig. 10 Effect of Re_ϕ on the radial distribution of Nu: $\lambda_T \approx 0.24$, $\beta_p \approx 1.0$

(β_p=0.5), where the heat transfer is governed by the boundary layer flow on the rotating disk. Here Nu increases with radius for $x > x_p$. For $x > 0.9$ there is a local peak in Nu. In this region the disk boundary layer fluid enters the receiver holes and there is a strong flow axially toward the disk, causing an increase in heat transfer coefficient.

At higher values of λ_T=0.24 and 0.36 (and the corresponding higher values of $\beta_p \approx 1.0$ and 1.2), the Nusselt number variation with radius is characterized by an inertial regime. The combined effect of increasing λ_T and β_p is greatest opposite the preswirl nozzles (x_p=0.74), where the more powerful preswirl flow at large λ_T impinges onto the disk. The Nusselt number decreases for $x_p < x < x_b$. The three-dimensional motion of the flow creates an increase in heat transfer coefficient near the receiver holes in all cases. In this region and outward of the receiver holes, Nu is less sensitive to λ_T and β_p.

Effect of Re_ϕ at Constant λ_T, β_p, and N=24. Figures 9–11 illustrate the effect of Re_ϕ on the radial variation of Nusselt number at fixed values of λ_T=0.12, 0.24, and 0.36, approximately, for which β_p=0.5, 1.0, and 1.2, respectively. For each fixed value of λ_T (and hence β_p) the magnitude of Nu increases with increasing Re_ϕ at all radii, but there is little effect of Re_ϕ on the *shape* of the Nu distribution. For the case characterized by the viscous regime (Fig. 9, $\lambda_T \approx 0.12$), the highest level of Nu is near the receiver holes. This local peak in Nu near the receiver holes occurs for all cases, but the maximum Nu is observed opposite the preswirl nozzles for cases with large β_p.

Effect of N and β_p at Constant Re_ϕ and λ_T. Figure 12 illustrates Nu distributions with radius for two experiments at common Re_ϕ and λ_T (hence common mass flow rate), but with different numbers of nozzles (N=12 and N=24) and hence different β_p.

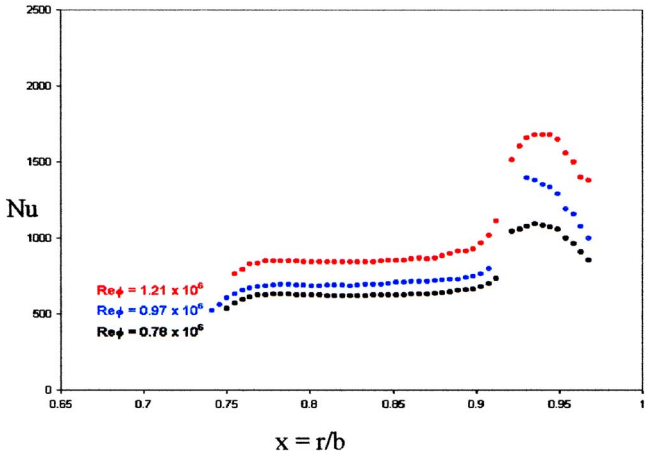

Fig. 9 Effect of Re_ϕ on the radial distribution of Nu: $\lambda_T \approx 0.125$, $\beta_p \approx 0.5$

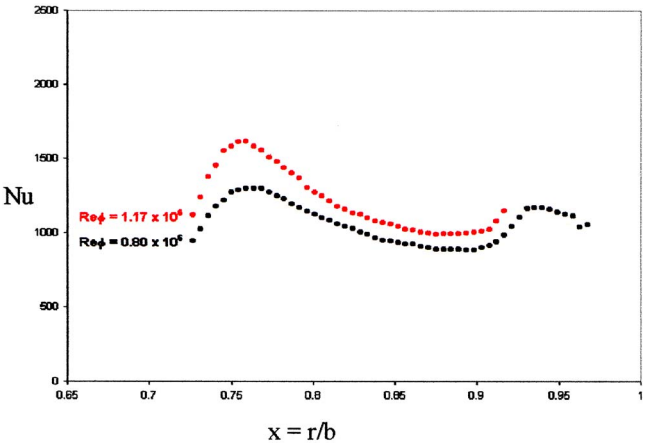

Fig. 11 Effect of Re_ϕ on radial distribution of Nu: $\lambda_T \approx 0.36$, $\beta_p \approx 1.2$

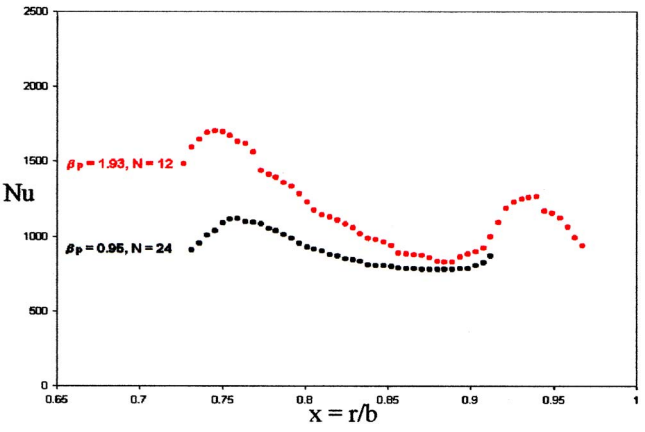

Fig. 12 Effect of β_p and N on radial distribution of Nu: $Re_\phi \approx 1.0 \times 10^6$, $\lambda_T \approx 0.24$

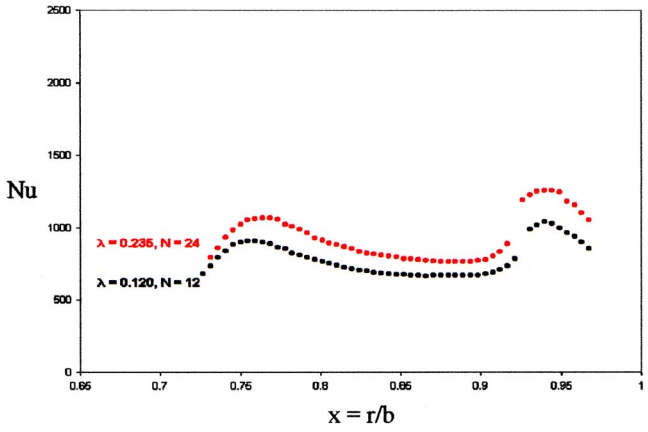

Fig. 13 Effect of λ_T and N on radial distribution of Nu: $Re_\phi \approx 0.8\times10^6$, $\beta_p \approx 1.0$

This figure clearly illustrates higher levels of Nu for the case $N=12$, which corresponds to greater nozzle jet velocities and impingement or inertial effects.

Effect of N and λ_T at Constant Re_ϕ and β_p. For a simple rotating-disk system, heat transfer on the disk is controlled by the development of the viscous boundary layer and this, in turn, is affected by the level of swirl outside the boundary layer $\beta_{p,m}$ [1]. Gord et al. [13] have shown that for constant β_p the level and distribution of $\beta_{p,m}$ is not sensitive to the number of nozzles N at the experimental conditions considered here. Figure 13 illustrates Nu distributions with radius for two experiments at common Re_ϕ and β_p, but with different numbers of nozzles ($N=12$ and $N=24$) and hence different λ_T. As the level of β_{pm} (which influences viscous effects) for these two cases is similar, these results suggest that increased inertial effects, for the higher mass flow rate at $N=24$, are mainly responsible for the increase in Nu. The uncertainty in the measurement of Nusselt number, based on the method described by Owen et al. [14], is estimated as ±5%.

7 Conclusions

An experimental study has been undertaken to investigate the influence of flow rate, swirl ratio, and rotational Reynolds number on the heat transfer in a rotor-stator system with preswirled air. Thermochromic liquid crystal (TLC), in conjunction with a stroboscopic light and digital video camera, has been used to obtain contour maps of Nusselt number Nu on the rotating disk in conditions featuring engine-representative flow structure.

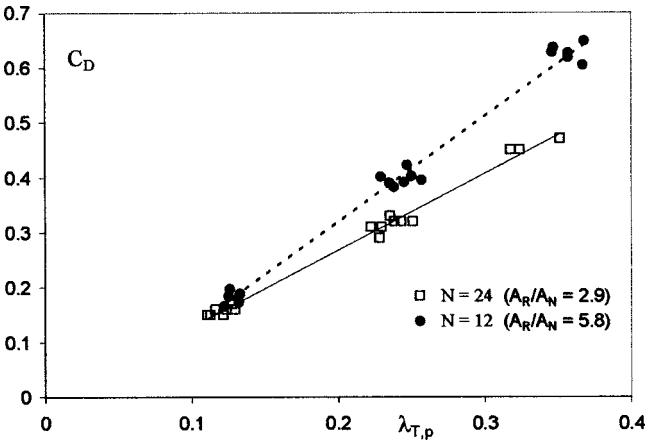

Fig. 14 Measured variation of C_D with $\lambda_{T,p}$ (corrected version of Fig. 8(*a*) of Yan et al. [9])

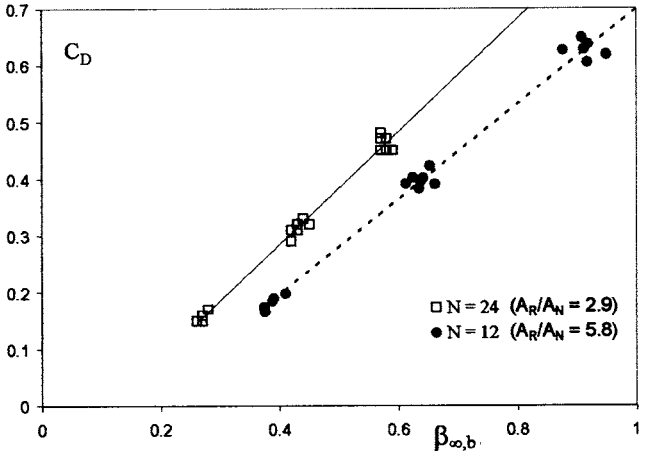

Fig. 15 Measured variation of C_D with $\beta_{\infty,b}$ (corrected version of Fig. 8(*b*) of Yan et al. [9])

Two heat transfer regimes were observed: a viscous regime at relatively low values of λ_T and an inertial regime at high values of λ_T. The viscous regime corresponds to axisymmetric boundary-layer flow over most of the rotating disk: for $x<x_b$, Nu increases as x increases. The inertial regime corresponds to impingement on the rotating disk around the preswirl nozzle radius, $x=x_p$. There is a peak in Nu near $x=x_p$ and, for $x_p<x<x_b$, Nu decreases as x increases; this behavior is also virtually axisymmetric.

Three-dimensional flow near the receiver holes on the disk creates nonaxisymmetric flow in this region, with large values of Nu between and around the holes. For both regimes, Nu increases as Re_ϕ, λ_T, and β_p increase.

Acknowledgment

This work was funded by Alstom Power Ltd. (now Siemens Industrial Turbines) and the UK Engineering and Physical Sciences Research Council. The authors are also grateful for the assistance of Dr. Y. Yan.

Nomenclature

a = inner radius of the disk
b = outer radius of the disk
c = specific heat of wall
c_p = specific heat at constant pressure of air
C_w = nondimensional mass flow rate ($=\dot{m}/\mu b$)
d = preswirl nozzle diameter
$f(\beta)$ = step-change solution of the Fourier equation
F = time-invariant adiabatic-wall parameter ($=T_{aw}-T_a$)
$g(\beta,\beta_\tau)$ = exponential solution of the Fourier equation
h = heat transfer coefficient [$=q_w/(T_{aw}-T_w)$]
k = thermal conductivity of wall
m = number of terms in exponential series
$\dot{m}$ = mass flow rate
Nu = Nusselt number [$=q_w r/k(T_{aw}-T_w)$]
q_w = heat flux from air to wall
r = radius from axis of rotation
Re_ϕ = rotational Reynolds number ($=\rho\Omega b^2/\mu$)
s = gap width
s_c = clearance spacing
t = time
T = temperature inside wall
T_a = total temperature of air
T_{aw} = adiabatic wall temperature
T_w = surface temperature of wall

x = nondimensional radius ($=r/b$)
β = parameter in step-change solution ($=h\sqrt{t/\rho ck}$)
β_p = preswirl ratio ($=V_{\phi,p}/\Omega r_p$)
β_τ = parameter in exponential solution ($=h\sqrt{\tau/\rho ck}$)
λ_T = turbulent flow parameter ($=C_{w,p}/\mathrm{Re}_\phi^{0.8}$)
ρ = density
θ = angle of preswirl nozzle to tangential
Θ = nondimensional temperature $[=(T_w-T_0)/(T_{aw,\infty}-T_0)]$
μ = dynamic viscosity
Ω = angular speed of rotating disk
τ = time constant

Subscripts

b = blade
e = exterior
j = jth term in series
m = outside the boundary layer
p = preswirl nozzle
o = value at $t=0$
s = seal
∞ = value as $t\rightarrow\infty$

Appendix: Corrected Measured Discharge Coefficients for the Paper by Yan et al. [9]

As explained by Yan et al. [9], corrections were made to the calculation of measured discharge coefficients C_D, compared to the conference paper version that appeared previously. The correct modified text was printed correctly in the journal version, however, the corresponding corrected figures were not. These corrected figures, which are consistent with the discussion in Yan et al. [9], are given in Figs. 14 and 15. In Ref. [10] the disk described in Figs. 7 and 8 should be described as rotating counterclockwise, not clockwise.

References

[1] Owen, J. M., and Rogers, R. H., 1989, *Flow and Heat Transfer in Rotating Disc Systems: Vol. 1, Rotor-Stator Systems*, Research Studies Press, Taunton, UK and Wiley, New York.
[2] Karabay, H., Wilson, M., and Owen, J. M., 2001, "Predictions of Effect of Swirl on Flow and Heat Transfer in a Rotating Cavity," Int. J. Heat Fluid Flow, **22**, pp. 143–155.
[3] Pilbrow, R., Karabay, H., Wilson, M., and Owen, J. M., 1999, "Heat Transfer in a "Cover-Plate" Pre-Swirl Rotating-Disc System," ASME J. Turbomach., **121**, pp. 249–256.
[4] Meierhofer, B., and Franklin, C. J., 1981, "An Investigation of a Pre-Swirled Cooling Airflow to a Turbine Disc by Measuring the Air Temperature in the Rotating Channels," ASME Paper No. 81-GT-132.
[5] Dittmann, M., Geis, T., Schramm, V., Kim, S., and Wittig, S., 2002, "Discharge Coefficients of a Pre-Swirl System in Secondary Air Systems," ASME J. Turbomach., **124**, pp. 119–124.
[6] Dittmann, M., Dullenkopf, K., and Wittig, S., 2003, "Direct Transfer Pre-Swirl System: One-Dimensional Modular Characterization of the Flow," ASME Paper No. GT-2003-38312.
[7] Geis, T., Dittmann, M., and Dullenkopf, K., 2003, "Cooling Air Temperature Reduction in a Direct Transfer Pre-Swirl System," ASME Paper No. GT-2003-38231.
[8] Chew, J. W., Hills, N., Kalatov, J. S., Scanlon, T., and Turner, A. B., 2003, "Measurement and Analysis of Flow in a Pre-Swirled Cooling Air Delivery System," ASME Paper No. GT-2003-38084.
[9] Yan, Y., Gord, M. F., Lock, G. D., Wilson, M., and Owen, J. M., 2003, "Fluid Dynamics of a Pre-Swirl Rotating-Disk System," ASME J. Turbomach., **125**, pp. 641–647.
[10] Lock, G. D., Yan, Y., Wilson, M., and Owen, J. M., 2003, "Heat Transfer Measurements Using Liquid Crystal in a Pre-Swirl Rotating-Disc System," ASME Paper 2003-GT-38123.
[11] Gillespie, D. R. H., Wang, Z., and Ireland, P. T., 1998, "Full Surface Local Heat Transfer Coefficient Measurements in a Model of an Integrally Cast Impingement Cooling Geometry," ASME J. Turbomach., **120**, pp. 92–99.
[12] Newton, P. J., Yan, Y., Stevens, N. E., Evatt, S. T., Lock, G. D., and Owen, J. M., 2003, "Transient Heat Transfer Measurements Using Thermochromic Liquid Crystal, Part 1: An Improved Technique," Int. J. Heat Fluid Flow, **24**, pp. 14–22.
[13] Gord, M. F., Wilson, M., and Owen, J. M., 2003, "Effects of Swirl and Flow Rate on the Flow and Heat Transfer in a Pre-Swirl Rotating-Disc System," IGTC2003 Tokyo TS-064.
[14] Owen, J. M., Newton, P. J., and Lock, G. D., 2003, "Transient Heat Transfer Measurements Using Thermochromic Liquid Crystal, Part 2: Experimental Uncertainties," Int. J. Heat Fluid Flow, **24**, pp. 23–28.